How to Quantify the Adsorption of Cyanuric Acid on Activated Carbon Used from Swimming Pool Disinfection?

Aneeshma Peter, Bénédicte Réty, Cyril Vaulot, Wajdi Heni, Thierry Steinbauer, Camelia Matei Ghimbeu

How to quantify the adsorption of cyanuric acid on activated carbon used from swimming pool disinfection?

Aneeshma Peter[a,b], Bénédicte Réty[a,b], Cyril Vaulot[a,b], Wajdi Heni[c], Thierry Steinbauer[c], Camelia Matei Ghimbeu[a,b*]

[a] Université de Haute-Alsace, Institut de Science des Matériaux de Mulhouse (IS2M), CNRS UMR 7361, F-68100 Mulhouse, France

b Université de Strasbourg, F-67081 Strasbourg, France

[c] WATERAIR swimming pools ZA Seppois-le-Bas, France 68580

*Corresponding author

Tel : +33 (0)3 89 60 87 43

E-mail: camelia.ghimbeu@uha.fr

Abstract

The physical and chemical characteristics of an adsorbent are key factors determining its efficiency in relation to a particular adsorbate molecule. The adsorption of cyanuric acid (cya) on activated carbon (AC) has not much been extensively explored in terms of its basic phenomenon and specific surface interactions. Cya is an important molecule in the swimming pool industry, as it protects free chlorine from UV light degradation. A proper characterization of AC will be beneficial for swimming pool product suppliers to determine the criteria while purchasing it to remove excess cya accumulated in pools. A detailed investigation of the physicochemical properties of activated carbon was conducted to assess its potential to adsorb cya from water. The effect of the adsorption capacity under various pH conditions was studied and it was found that acidic pH favors the adsorption process. With the help of temperature-programmed desorption coupled with mass spectrometry (TPD-MS) and X-ray photoelectron spectroscopy (XPS), the surface chemistry was well analyzed for a proper understanding of the adsorbent-adsorbate interaction. While conventional pool test equipment gives inconsistent readings of the cya concentration, a UV-vis spectroscopy-based methodology has been developed to accurately measure traces of cya in water. This method can be helpful to validate the accuracy of pool-testers for research and development purposes. The batch adsorption experiments revealed that cya adsorption on activated carbon follows pseudo-second order kinetics, which confirms that the adsorption mechanism is chemisorption, which in fact, depends highly on the surface chemistry of the AC and the reaction pH.

Keywords: Activated carbon; cyanuric acid; physicochemical properties; pH; adsorption kinetics; UV-Vis spectroscopy

Introduction

Diseases caused by waterborne infections are rapidly spreading illnesses caused by bacteria and viruses. One of the localities where the spread can occur exponentially is swimming pools, and thus, disinfecting the water of swimming pools is essential while maintaining the quality of the water[1,2]. The most common and inexpensive method for this purpose is to chlorinate water using sodium hypochlorite (NaOCl), calcium hypochlorite (Ca (OCl) 2), or other derivatives such as chloroisocyanurate[3]. This is intended to prevent recreational water infection, suppress the activation of pathogenic microorganisms, and avoid waterborne diseases. However, in the case of outdoor pools, studies have shown that in sunlight 75-90% of chlorine can be wiped out in two hours[4]. In addition, ultraviolet (UV) radiation from sunlight can also contribute to the degradation of hypochlorous acid (HClO) into hydrochloric acid (HCl). Therefore, in swimming pools, a chlorine stabilizer is used to protect chlorine molecules from degradation and to effectively serve as a disinfectant. Cya is a common compound in the swimming pool industry and serves as a protection shield for chlorine against sunlight[5].

Although there are no relevant studies to prove severe health hazards related to cya exposure, the conventional pool industry suggests an ideal cya range of 30-50 ppm, with a minimum of 10 ppm and a maximum of 100 ppm. Chloroisocyanurates are compounds commonly used in outdoor swimming pools to stabilize chlorine disinfectants. The chloroisocyanurates slowly decompose to release chlorine, which serves as a disinfectant, and cya as a stabilizer, both at the same time. However, this sanitation method results in a build-up of cya with time. One of the most common chlorine derivatives of cya is trichloroisocyanuric acid (TCCA). For each gram of TCCA, 0.55 grams of cya are formed in the water. If the amount of cya in a pool exceeds its allowed level, it can bind to the chlorine molecules present in the system and reduce its effectiveness in killing algae and other bacteria in the water [6]. This phenomenon is commonly known as the 'chlorine lock' in the swimming pool industry. Thus, excessive

concentrations of cya should be avoided, in order to ensure disinfection but also to circumvent algae growth.

However, the maximum recommended concentration of cya to be used in pools has been debated for decades because it is difficult to determine at what point the reduction in HOCl activity becomes an unacceptable public health risk. Falk et al. [7] studied the impact of cya on the risk of gastrointestinal illness among bathers in swimming pools and stated that reductions in infection risk can be achieved by reducing the allowed cya/Free Chlorine ratio.

One of the commonly used methods to remove excess cya from swimming pools is by using activated carbon filters. The availability, low cost, and unique structural and surface properties of activated carbon make it an interesting candidate to capture the cya present in pools and restrict its accumulation.

The first limitation is that there are no studies available in the literature that evaluate the adsorption of cya on activated carbon. The main reason could be the complex analysis of cya in a liquid medium. However, looking at the chemical structure of cya ($C_3H_3N_3O_3$) and the surface properties of activated carbon, we can estimate possible interactions that occur when they are in contact. The molecular size of cya is approximately 0.65 nm (approximate calculation using Webmo[8]). If the porosity of activated carbon is characterized, the possibility of capturing these molecules based on physisorption reactions can be estimated.

The chemical structure of cya (containing N, -OH groups) could favor physical adsorption on the activated carbon sites. However, the efficiency of this adsorption process will depend on the nature of the activated carbon surface. The presence of hydrogen and oxygen atoms in the molecular structure of cya can also contribute to hydrogen bonding with the oxygenated surface functional groups of activated carbon. Sigmund *et al.* indicated that aromatic compounds such as phenols increase their adsorption capacity if π–π interactions occur between the

adsorbate and adsorbent[9]. This is promising evidence that the cya molecule can also be adsorbed on activated carbon because of its structure with aromatic rings. Therefore, the proper characterization of activated carbon materials is essential to evaluate their efficiency as adsorbent for cya in swimming pools.

The quantification of the cya molecule is often complicated, mainly due to the structural tautomerism exhibited when exposed to water [10,11]. For swimming pool applications, pool-tester equipment is used to measure the amount of cya because of its simple operating method. This measurement of cya is based on the turbidity level, which is caused by the complexation of melamine-containing cya test pills with cya[12]. The literature shows that this melamine cyanurate precipitation method with the spectrophotometric determination of turbidity is comparatively less precise (error of ±10 ppm) than methods such as liquid chromatography, but still a useful method if correctly validated[13]. However, the precipitation method has been found to have a limited sensitivity in the range of 10-50 mg/L. More sophisticated analytical techniques, such as high-performance liquid chromatography (HPLC) and UV-vis spectroscopy, and other spectroscopic techniques, have been implemented in various works to detect the amount of cya [14–16]. However, the higher operating cost limits the application to real-life purposes. In 1947, Irving *et al.* had studied the absorbance spectra of cya, and they highlighted the tautomerism of cya in solution [10]. As discussed above, within solution, cya exists in a triol form (-OH) and keto form (=O) in an equilibrium state (Figure S1). Depending on the solution preparation conditions (pH, initial concentration, temperature etc.), this equilibrium can be shifted to its favorable side. If the pH of the solution is increased above 7.5, the forward reaction will be favored, and the non- UV absorbing keto form of cya will change to the triol form, which is strongly UV-absorbing molecular form. The reason behind this strong absorbance is its anionic resonance structures. The resonance in such systems gives rise to a structure that may be the ground state for a transition corresponding to the absorbance at

220 nm. The minimum pH should be kept at 7.5 to achieve this absorbance[10]. Hence, if the pH of the liquid medium is controlled at the desired level, cya could be measured more accurately using spectroscopy.

Another interesting technique to identify and quantify adsorbed molecules on carbon materials is temperature program desorption coupled with mass spectrometry (TPD-MS). This technique has already been used in previous studies to quantify various organic molecules such as chlorinated compounds and hydrocarbons[17,18]. This technique not only allows qualitative and quantitative analyses, but also provides information on the interaction between the adsorbent and the adsorbate molecule, depending on the temperature at which the molecule is desorbed and the fragments of decomposition of the molecule[19]. It also provides insight into the interactions between the surface groups of carbon materials and a specific molecule. In fact, surface groups can give selective adsorption properties[20]. Therefore, TPD-MS could be a promising analysis technique for identifying and quantifying adsorbed cya on AC. It is worth noting that no previous studies have used TPD-MS for this purpose.

In this paper, we study the physicochemical properties of a commercially available activated carbon and examine whether the characteristics are suitable for the efficient adsorption of cya from water. The influence of the reaction pH is also investigated to assess the difference in adsorption capacities. The detection limit and inconsistency of pooltester equipment are validated using a developed methodology based on UV-vis spectroscopy, which is highly dependent on the pH of the solution. Understanding the basic adsorption mechanism along with the proper characterization of activated carbon can be useful for the swimming pool industry in choosing the appropriate activated carbon filter for the removal of cya. An optimized pH condition and quantification method can also be beneficial in enhancing the efficiency of cya adsorption procedures in swimming pools.

Experimental

Activated carbon and characterization

A commercial activated carbon was used in this study. The morphology and the composition of the materials were examined by Scanning Electron Microscopy (SEM) from Philips model FEI Quanta 400, equipped with an Energy Dispersive X-Ray (EDX) analysis. To obtain the contact pH of the material, AC was mixed in deionised water at a 1:20 mass to volume (g mL^{-1}) and stirred at room temperature for 72 h [21]. The pH of the reaction mixture was then directly measured using Metrohm STAT Titrino pH-meter.

The textural properties of the materials were investigated from the adsorption isotherms of N_2 at 77 K and CO_2 at 273 K using Micromeritics ASAP 2420 instrument. Prior to analysis, the samples were outgassed overnight under vacuum at 300 ° C. The BET specific surface area (S_{BET}), was calculated in the relative pressure range p/p_0 of 0.01 to 0.05 for N_2 and 0.01 to 0.03 for CO_2 from the adsorption. The total pore volume (V_p), the volume of micropores (Vmicro), the volume of mesopore (Vmeso) and the volume of ultra-micropores ($V_{ultramicro}$) were calculated as described in the SI. The pore size distribution was determined using the NLDFT models SAIEUS programme by Jacek Jagiello)[22] . The water vapour adsorption isotherm was obtained at 25 ° C using Micromeritics Triflex, to understand the hydrophilic/hydrophobic nature of activated carbon.

Bruker D8 Advances X-ray diffractometer was used to determine the possible phases and presence of crystalline impurities in the activated carbons, using a Cu-K α radiation (ʎ = 0.15406 nm).

Thermogravimetric analysis (TGA) was performed using Mettler-Toledo TGA 851e to understand the thermal stability of activated carbon. The analysis was carried out under N_2 with a flow rate of 100 mL min^{-1} with constant heating from 30 to 900 ° C at 5 °C min^{-1}. The amount of ash was determined by heating the sample at 900 °C for 1 h under air [20,23].

TPD-MS was used to determine oxygenated surface functionalities on AC and to measure the cya desorbed from the carbon surface [17,20,24,25]. In a typical TPD-MS experiment, the samples are placed in a quartz tube in a furnace and heat-treated with a linear heating rate under secondary vacuum. Gases evolved during the heating process are continuously quantitatively analysed by a mass spectrometer. The amount of various gases desorbed during heating provides information about the surface functional groups present on the material and the adsorbed species. To evaluate the surface chemistry of activated carbons and to study the desorption of oxygenated surface groups, we used a homemade TPD-MS setup with a heating rate of 5 °C min^{-1} in the temperature range 25-950 °C.

The total pressure of the gas released during heat treatment was measured as a function of the temperature. This total pressure was then compared with the sum of the partial pressure of the species deduced from the mass spectrometer measurement and the calibration of several gases (CO (m/z=28), CO_2 (m/z=44), H_2O (m/z=18), H_2 (m/z=2), performed prior to the measurement. The pressure profile measured by the gauge and the pressure profile recalculated from the partial pressures overlap if the gases released during the measurement are calibrated gases. On the contrary, when a difference between the two pressure profiles (measured and calculated) is observed, it indicates the presence of one or several non-calibrated gases. By correlating the mass intensities, the measured pressure, and the calibration data, the desorption rate of each gas (mol s^{-1} g^{-1}) can be calculated for the calibrated gases. In addition, the total amount of each calibrated gas can be calculated by time integration of the desorption rate versus the temperature curves.

Batch adsorption experiments

Commercially available cya powder Aquastab, purchased from Lawrason's, Inc. containing 80-100 % cya was used to prepare the solutions. In a typical assay, 1000 mg of L^{-1} stock solution

of cya was prepared by dissolving an appropriate amount of Aquastab in tap water and stirring for 2 h at room temperature to ensure complete solubilization. The required concentrations were freshly prepared from this stock solution for each adsorption batch. The pH of the cya solution ranged from 7 to 7.5 depending on the pH of the tap water. Adsorption experiments were carried out in 100 mL dilution bottles with 150 mg L^{-1} adsorbent. Activated carbon was mixed in a solution of 125 ppm cya by agitating on a reciprocating shaker at 25 ° C at ~ 125 rpm to ensure proper mixing of AC with the solution. The samples were kept for 4 days to guarantee saturation, after which the solution was vacuum filtered using Whatman filter paper, and both the liquid (containing cya) and solid (AC) fractions were recovered for further analyses. The initial and final concentrations of cya was used for calculations.

At least 3 batches were performed for each experiment to assess the repeatability with minimum standard deviation.

Liquid phase analysis after adsorption

Pooltester measurements

Pooltester equipment from Lovibond was used to measure the amount of cya in the solution. Cya measurement is based on the turbidity level that is caused by the complexation of melamine-containing cya test pills with cya. The cya test pills were placed in the filtrate and thoroughly dissolved with 1 min of vigorous shaking. The readings were taken after 5 min to ensure a consistent value. A minimum of 3 batches were performed and average yield values are reported with standard deviation. For each batch, cya-tests were performed in triplicate, and average values were used to calculate adsorption capacity. Readings that are completely different from the expected concentration range that could be caused by insufficient dissolution of the pill were omitted for better comparison.

First, the residual cya concentration in the filtrate was measured using a pooltester. The amount of adsorbed cya, Q (mg g^{-1}), was calculated using Eq. 1.

$$\text{Adsorption capacity, } Q = \frac{(C_{initial} - C_{final})}{m} * V \quad (1)$$

Where Q is the adsorption capacity (mg g^{-1}), $C_{initial}$ is the initial concentration of the adsorbate (mg L^{-1}), C_{final} is the final concentration of the adsorbate (mg L^{-1}), V is the volume of solution (L), and m is the mass of the adsorbent (g).

As this method is sometimes inaccurate, other methods such as UV-VIS and TGA have been proposed as alternative methods that can be used by swimming pool suppliers. Furthermore, more sophisticated techniques such as TPD-MS and XPS were employed to better understand the interactions of carbon with the cya.

UV-Vis spectroscopy

For kinetic experiments, the UV-Vis method was used. The samples were removed and filtered at the desired time intervals (0.5, 1, 2, 4, 8, 16, 24, 48, and 72 h). Experimental data were fitted to linear forms of pseudo first order (Eq. 2), pseudo second order (Eq. 3) and intra-particle diffusion (Eq. 4) kinetic models[26] .

$$\log(Qe - Qt) = \log Qe - \frac{k_1 * t}{2.303} \quad (2)$$

$$\frac{t}{Qt} = \frac{1}{k_2 * Qe^2} + \frac{t}{Qe} \quad (3)$$

$$Q_t = k_{ip} * t^{0.5} + C \quad (4)$$

Where Q_t and Q_e (mg g^{-1}) are adsorbed amounts at time t (minute) and equilibrium respectively, and k_1, k_2 and k_{ip} are the rate constants for the pseudo first order, pseudo second order and intra particle diffusion kinetic models, respectively. The rate constant k quantifies the rate and direction of a chemical reaction. The best fit model was determined by the regression factor R^2

to understand the mechanism of adsorbent-adsorbate interaction. Slope and intercept values were used to calculate Q_e and rate constant, k.

A UV-Vis spectrophotometer Lambda 750 was used to determine the amount of cya adsorption at an absorbance corresponding to a wavelength of 213 nm (Figure S2a). The calibration curve was obtained (Figure S2b) using known concentrations of cya in the range of 20 to 100 mg L^{-1}, maintaining a pH of 8. The amount of cya adsorbed at 213 nm was calculated using Beer-Lamberts equation.

Each reading was taken in triplicate and the average value is reported.

Diluted HCl (36 %) and NaOH purchased from Carlo Erba reagents and pH = 6 and pH= 8 buffers purchased from Sigma Aldrich were used for pH corrections.

Solid phase analysis after adsorption

Thermogravimetric analysis

TGA was also used to quantify the amount of adsorbed cya inside the AC. Samples were heated from 30 to 900 °C at a rate of 5 °C min^{-1} under a nitrogen atmosphere. The weight loss occurring in the temperature range between 200 and 400 °C, labelled as WL_2, was determined from Origin plots. Each measurement was repeated at least 3 times to check the consistency and average values are reported.

TPD-MS analysis

TPD-MS analysis was performed to confirm the nature of the adsorbed compound on activated carbon in the WL_2 temperature region. The difference in calibrated and measured pressure profiles from the TPD-MS data was used to identify the decomposition temperature of the adsorbed molecule. This difference is caused by the uncalibrated gases that are desorbed from activated carbon at this particular temperature. Uncalibrated peaks corresponding to gases

evolved at this temperature were extracted from TWare32 software and compared with theoretical MS spectra of expected molecules.

XPS analysis

To analyse and quantify the surface functionalities on carbon surface, high resolution X-ray Photoelectron Spectroscopy (XPS) data were obtained on a SCIENTA 200 X-ray photoelectron spectrometer equipped with a conventional hemispherical analyser.

Results and discussion

Physical and chemical properties of activated carbon

To understand the nature of the surface of AC at a microscopic level, surface morphology analysis was performed using scanning electron microscope images. Figure. 1a compares images of activated carbon obtained at different scales. It was observed that the activated carbon surface was smooth, homogenous but small white dots on the surfaces are visible, which could be related to the presence of inorganic impurities.

The approximate particle size was calculated using the SEM images on a 1mm scale with the help of ImageJ software and was found to be 2.15 mm on average. This large particle size will be an advantage because it helps to reduce the dust pollution inside the pools and prevents the dispersion of particles from stored bags.

The pH measurements revealed that the activated carbon had a pH of 8.1 which indicated the presence of a negatively charged surface, possibly due to oxygenated functionalities, which could be favorable for cya adsorption. To further confirm the presence of oxygen and other elements present on the surface, the elemental composition of the surface was determined by EDX analysis (Figure S3 and Table S1).

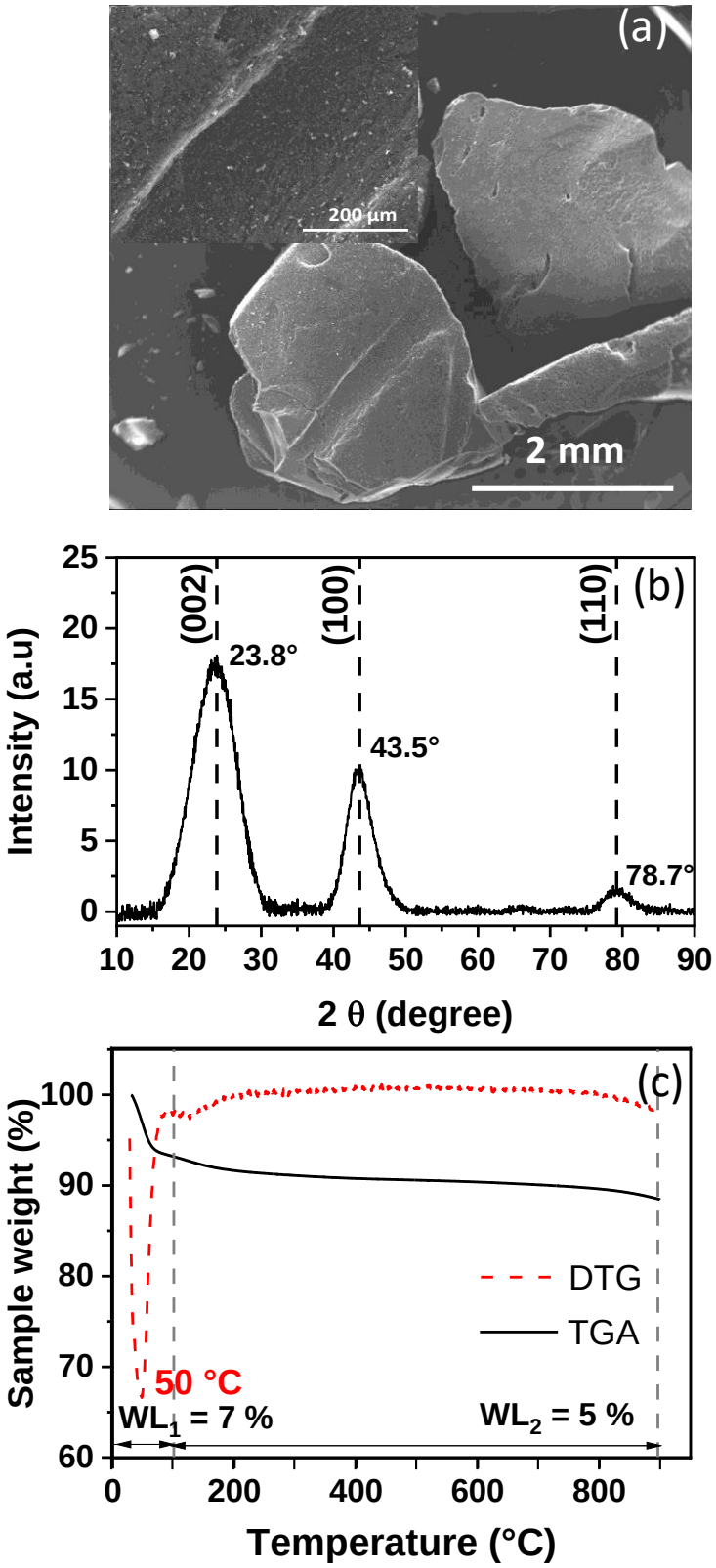

Figure 1. (a) SEM images of activated carbon at 2 mm scale (in set 200 µm scale), (b) XRD pattern of activated carbon after the baseline correction and (c) thermal decomposition of activated carbon profile and the derivative curve by TGA.

The AC Contains an average of ~ 80 at. % of C, 15.5 wt% of O and a total amount of impurities (K, Ca, Si, Mf etc.) of ~ 5.27 at%. These values were obtained as an average of three measurements performed in different areas on the carbon surface.

The XRD pattern of activated carbon (Figure 1b) shows a large peaks at 23.85° and 43.52° corresponding to (002) and (100) planes of graphite, respectively[27], typically for a disordered structure with a low degree of graphitisation . No peaks related to the inorganic impurities were noted, probably because of their possible amorphous nature. However, the presence of such mineral impurities (K, Ca, Mg, Si etc) is typically associated with the ash content of the sample, therefore, based on TGA weight loss by heating the sample at 900 °C under air for 1 h (Figure S4) a very low content was determined (~ 1.2 %). The TGA weight loss profile for AC along with its derivative curve, carried out under a N_2 atmosphere up to 900°C, is represented in Figure 1c. A significant weight loss (WL_1 = 7 wt%)) at a temperature of approximately 50 °C corresponding to the decomposition of physisorbed water is seen. This shows the moisture affinity of activated carbon which could be due to a high porosity or richer surface chemistry. A gradual weight loss (WL_2 = 5 wt%)) in the higher temperature region was observed, which could be related to the degradation of functional groups on the surface, as will be shown later by TPD-MS.

The nitrogen adsorption-desorption isotherms are depicted in Figure 2a. Activated carbon followed the type I isotherm characteristic to microporous materials with relatively high external surface area (990 $m^2 g^{-1}$). The textural properties are given in Table 1.

Table 1. Textural properties of activated carbon based on N_2 and CO_2 adsorption

Property	S_{BET} ($m^2 g^{-1}$)	V_{micro} ($cm^3 g^{-1}$)	V_{meso} ($cm^3 g^{-1}$)	$V_{ultramicro}$ ($cm^3 g^{-1}$)	Average pore diameter L_0 (nm)
Activated carbon	990	0.38	0.06	0.29	0.76

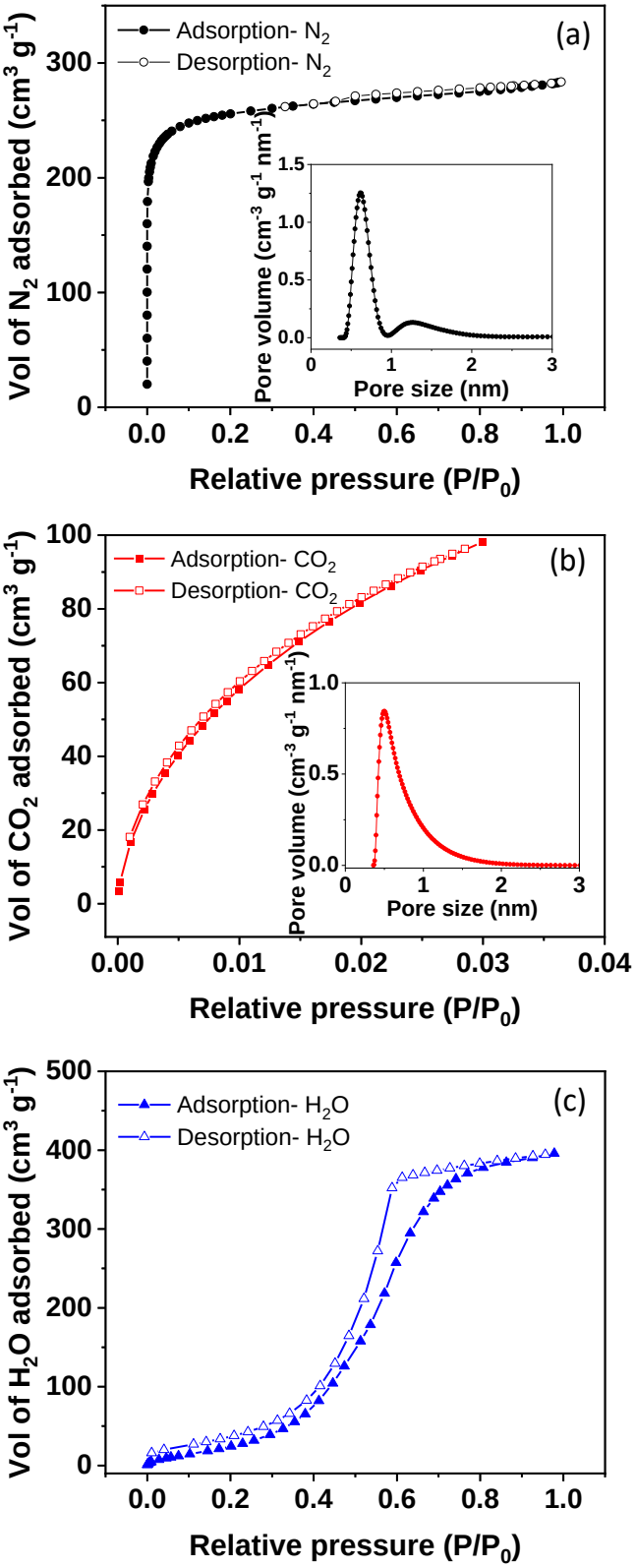

Figure 2. Adsorption/desorption isotherms for activated carbon (a) Nitrogen at 77 K with NLDFT pore size distribution inset (b) CO_2 at 273 K with NLDFT pore size distribution at micopore region and (c) H_2O at 289 K

The pore size distribution determined using NLDFT model along with N_2 adsorption isotherm (inset Figure. 2a) shows the main pore size distribution approximately 0.5 nm with a small contribution of 1.5 nm, while. the average pore diameter, L_0 is 0.76 nm. Considering the size of cya adsorbate (0.65 nm), we can assume that some of these pores provided restricted access to cya because of their size while the accessibility of the adsorbate molecule could be higher in larger micropores and mesopores. However, the fraction of mesopores was rather low (0.06 $cm^3\,g^{-1}$).

To validate these micropore characteristics, the values of $V_{ultramicro}$ were determined by the CO_2 adsorption isotherm and 2D-NLDFT pore size distribution (Table 1, Figure 2b). These results indicated the presence of small pores (mean size ~ 0.5 nm) in the material.

The water adsorption isotherm (Figure 2c) can be used as an indicator of the affinity of activated carbon for moisture. The isotherm presented a type IV sigmoidal shape that is generally observed due to secondary adsorbate–adsorbate interactions, such as capillary condensation in mesopores. The S_{BET} value for water adsorption for activated carbon was determined to be 462 $m^2\,g^{-1}$. In the adsorption process, the functional groups of the carbon surface are of great importance because of their interactions with the molecules to be adsorbed. The type and quantity of these surface oxygenated groups were determined by temperature-programmed desorption. The oxygen surface groups decompose with the evolution of CO and CO_2 gases. The nature of the evolved gases and the evolving temperature provide an indication of the nature of the functional groups. CO_2 has been shown to come from groups such as carboxylic acids, anhydrides, and lactones while CO comes from groups such as phenol, carbonyl or quinone[28,29]. The pressure profile of AC and the amounts of CO, CO_2, H_2, and H_2O are shown in Figure 3b. We can see that the pressure profiles overlapped (Figure 3a), indicating that activated carbon only released calibrated gases and that there were no unknown gases released.

A high hydrogen release above 800 °C corresponded to cleavage of the unsaturated C-H bonds. The H_2O profile exhibited a large peak of physisorbed water at approximately 100 °C. The release of CO_2 in the range of 100-400 °C indicated the presence of carboxylic functional groups. The intense peak of CO around 800 °C corresponded to phenolic, carbonyl and ether groups. The TPD profiles confirmed the presence of acidic functionalities on the activated carbon surface, which will be advantageous for the possible interaction with cya.

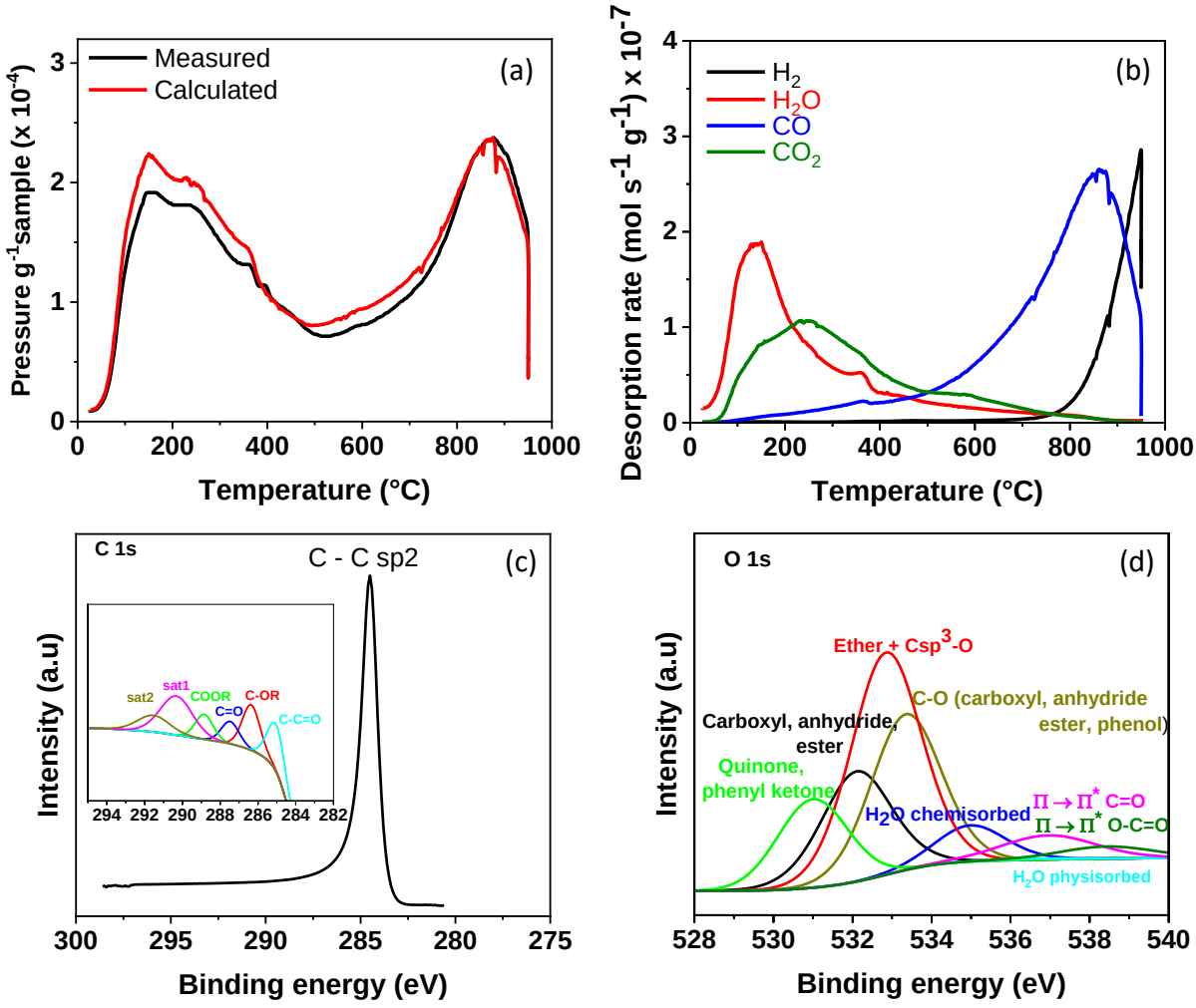

Figure 3. TPD-MS analysis of activated carbon (a) Measured and calibrated pressure profiles and (b) Amount of calibrated gases desorbed from the AC surface; high resolution XPS spectra of (c) C1s and (d) O1s.

Based on XPS survey spectra the atomic percentage of surface carbon and oxygen content were approximately around 94 at.% and 5 at. % . The high-resolution spectra of C1s and O1s (Figure 3c, d) were used to quantify the type and amount of functional groups on the extreme carbon surface (~10 nm). The specific binding energy of 284 eV was assigned for C 1s (Figure 3c) corresponding to non- functionalized carbon (sp2 and sp3 hybridized) belonging to C-C/C-H bonds of the carbon skeleton. The O 1s peak at 532 eV corresponds to the surface functionalities (Figure 3d)

Both peaks showed that the nature of the functionalities were acidic and major groups represented on the carbon surface include -COOR, C=O, C-OR and C-C=O. The results were in good agreement with the TPD-MS analysis.

The physicochemical characterizations revealed that activated carbon exhibited a generally suitable surface property that could be favorable for cya adsorption. Appropriate S_{BET}, ultramicropore volume, particle size, and amount of acidic surface functionalities will be helpful for H-bonding with Cya and other possible surface interactions. When the pore size is close to the cya molecule size the adsorption is expected to be favored, and mesopores may favor the diffusion process[30–32].

Adsorption behavior of cya on activated carbon

To evaluate the adsorption capacity of activated carbon for cya, batch adsorption experiments were conducted using an initial adsorbate concentration of 125 ppm. Eq. 1 is used to calculate the adsorption capacity in mg g^{-1}. Activated carbon was found to have an adsorption capacity of 88.1±19.9 mg g^{-1}. Pooltester readings were utilized with at least 3 batches to obtain a minimum standard deviation (Table 2). There was still some inconsistency between the batch measurements.

As an alternative method, a weight loss calculation using the cya TGA decomposition profile was also implemented and is represented in Figure 4a.

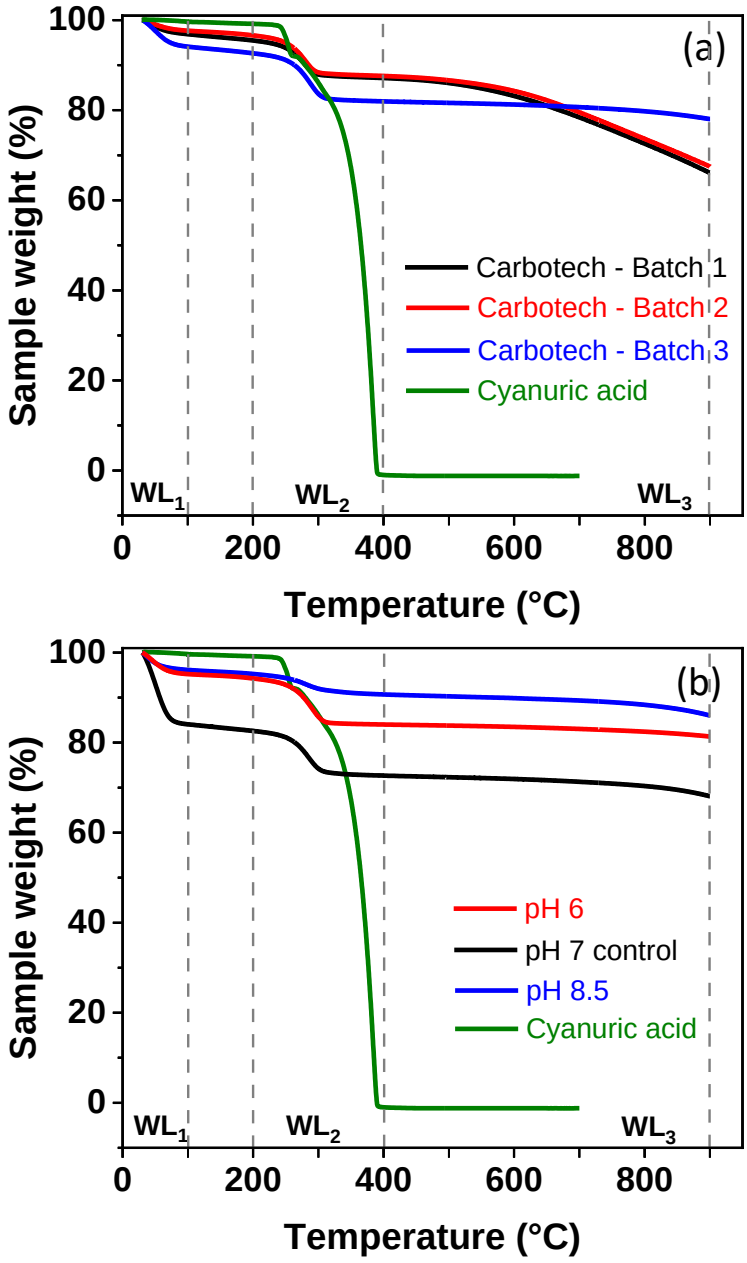

Figure 4. (a) TGA weight loss comparison between different batches of activated carbon after cya adsorption and (b) TGA weight loss comparison after cya adsorption under different conditions of pH

The main decomposition of cya occurred in the temperature range between 200 – 400 °C (WL_2). Meanwhile 0 – 100 ° C is defined as WL_1 where volatile and moisture decomposition occurred and 400 – 900 ° C is defined as WL_3 where functional decomposition occurs predominantly. The amount of cya adsorbed on activated carbons after the adsorption tests, was calculated based on its thermal decomposition within this temperature range, i.e., at WL_2. Furthermore, to compare this calculated value of cya from TGA with the pooltester results, the adsorption capacity determined based on Eq. 1, was converted to the yield of adsorption, following Eq. 5. This equation was obtained by slightly modifying Eq. 1 and converting to a percentage value.

$$Adsorption\ yield = \frac{\Delta\ Cya\ *\ V}{\mathbf{1000}\ *\ Wt_{AC}} * \mathbf{100} \tag{5}$$

Where $\Delta\ Cya$ is the change in cya concentration (mg L^{-1}), V is the volume of solution (L) and Wt_{Ac} is the mass of adsorbent used for tests (g).

Table 2 compares the cya quantification results based on the pooltester yield (Eq. 5) and TGA method. It was interesting to observe that the pooltester yield percent and WL_2 gave almost similar values for cya adsorption (8.8±2.4 *vs.* 9.5 ±0.9). The agreement between the two quantification methods was s rather good, however, the values obtained by the pooltester had higher standard deviations than those obtained by TGA.

The results of these experiments demonstrated that TGA weight loss in the 200-400 °C temperature range could be used to monitor the change in cya concentration in swimming pools. Considering the inconsistent results from the pooltester, the TGA method could be an alternative, easy and cost-effective method to quantify the cya. .

Table 2. Comparison of cya adsorption quantification using the pooltester and TGA weight loss methods

Batch	Batch 1	Batch 2	Batch 3	Average
Adsorption capacity, Q (mg/g) (Pooltester, Eq.1)	60	104.4	100	88.1 ± 19.9
Adsorption yield (%) (Pooltester, Eq.6)	6	10.4	10	8.8 ± 2.4
WL_2, wt. % (200-400 °C) (TGA)	8.6	9.4	10.4	9.5 ± 0.9

Effect of solution pH on the adsorption of cya on activated carbon

To understand the influence of different pH conditions on the adsorption of cya, batch adsorption experiments were performed by varying the pH of the reaction mixture. Typical pH values of swimming pools are between pH 6 and 8.5.. Because the normal reaction pH of the adsorption batches is between 7 and 7.4, the reaction pH was varied to 6 and 8.5 using diluted HCl and NaOH, respectively, to evaluate the effect of pH on the adsorption of cya. The results are given in Table 3.

Table 3. Comparison of cya adsorption quantification using the pooltester and TGA weight loss methods under different pH conditions

Batch	pH 6	pH 7 control	pH 8.5
Adsorption capacity, Q (mg/g) (Pooltester, Eq.1)	166.7 ± 15.8	72 ± 5.5	123.5 ± 20.3
Adsorption yield (%) (Pooltester, Eq.6)	16.7 ± 1.5	7.2 ± 0.6	12.3 ± 2.1
WL_2, wt. % (200-400 °C) (TGA)	10.6 ± 0.7	8.3 ± 1.7	5 ± 0.5

It is interesting to note that the acidic pH increased the adsorption yield to 16.7%, which is nearly two times higher than that of the pH 7 control (7.2 % adsorption yield). This indicated that the acidic pH influenced the adsorption of cya, possibly by activating the surface functionalities in favor of cya adsorption. The cya yield for pH = 8.5 was also improved to 12.3 %, indicating favorable adsorption at basic pH as well. However, the TGA profiles for these samples (Figure 4b) showed that the value of WL_2 was much lower than the adsorption yield calculated by the pooltester (Table3). The samples performed at acidic pH showed slightly higher weight loss in the WL_2 region (10.6%) than the other two pH levels, indicating an improvement in the adsorption capacity. A clear trend was identified with pH, i.e., by lowering the pH, the weight loss corresponding to cya decomposition increased.

Notably, the TGA decomposition profiles were consistent for all 3 batches and the standard deviation was very low (< 1%). The observed difference between the TGA weight loss and pooltester yield methods could be due to the effect of pH on the pooltester measurements. More precisely, we observed that the solubility of the cya test pill differed at various pH values. Therefore, proper mixing of the cya test pills in the cya filtrate should be ensured during practical applications.

TPD-MS analysis was performed to confirm that the adsorbed compound on activated carbon in the WL_2 temperature region was cya and compare its relative adsorbed quantity. The pressure profile of the TPD-MS and the desorption profiles of the uncalibrated peaks as a function of temperature are represented in Figure 5 for samples performed under various pH conditions.

First, a large release of gases can be observed in the temperature region of 200-350 °C, in good agreement with the TGA results. The calculated and measured pressures (Figure 5a-c) during

the temperature ramp are significantly different at approximately 275 °C, indicating that an unidentified molecule is desorbed at this particular temperature.

As seen in Figure 5d-f, the set of m/z peaks that emerged from this molecule corresponded to the theoretical MS spectra of cya (Figure S5). At 275 °C, the peak at m/z = 43 as the most intense for all materials, and this was also present in the theoretical spectra of cya. Therefore, the peak at 43 could be used as the characteristic peak of cya for further analysis. For the pH 6 and pH 7 control samples, this peak appeared to be almost similar in intensity, while for pH 8.5 all m/z peak intensities were relatively low. This observation agreed well with the TGA WL_2 values, where a slight increase in cya adsorption was observed for pH 6 samples and a significantly low adsorption for the pH 8.5 samples.

Figures 6 (a) and (b) show the TPD-MS profiles of CO (m/z=28) and CO_2 (m / z = 44). Due to the desorption of cya at 280 °C temperature region, the CO and CO_2 peaks were mainly due to the contribution of the intensities of the secondary peaks of the decomposition of cya. However, above 400 °C, where the measured and calculated pressure curves overlaped (Figure 5), the CO and CO_2 profiles were representative of these calibrated gases, so the total calibrated gases quantities plotted in Figure 6 (c) are given between 400 °C and 950 °C. The CO_2 evolved above 400°C was low but slightly t higher in intensity for pH 6 in comparison to the other samples.

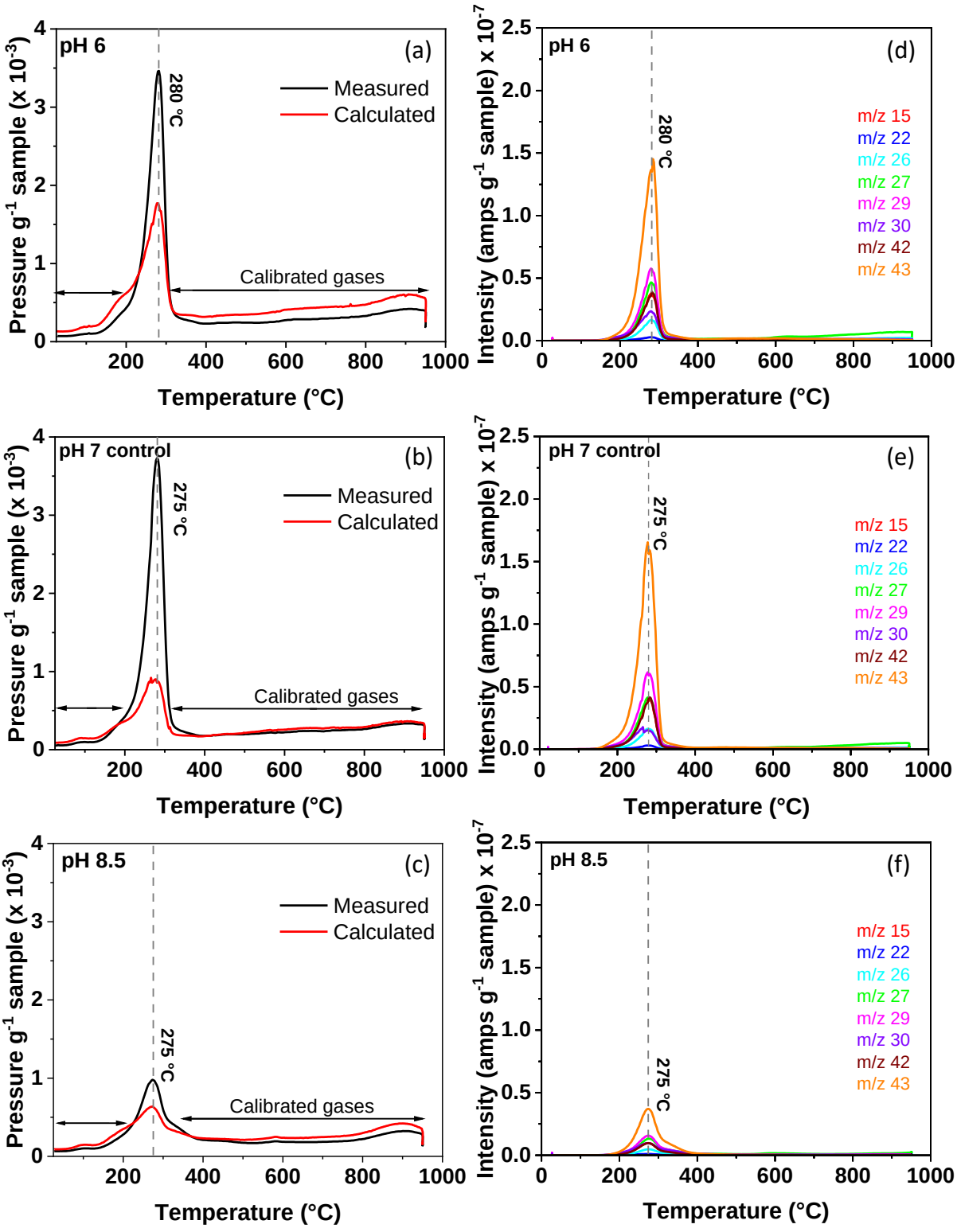

Figure 5. TPD-MS analysis of activated carbons after adsorption of cya under different pH conditions. Pressure profiles at (a) pH 7 control (b) pH 6 and (c) pH 8.5. Mass spectra of the uncalibrated species (d) at pH 7 (e) at pH 6 and (f)at pH 8.5

The CO desorption profiles of the pH 7 samples and the pristine AC, above 400°C, were similar. The CO released between 600 and 950 °C may have been due to the decomposition of the surface groups of phenol, ether, carbonyl, and quinone surface groups[33,34]. The sample pH 6 exhibited a similar profile trend, but with a higher intensity at 900°C, which could be due to more of these functional groups. Unlike the pH 8.5 sample, the pH 6 sample, showed a higher CO release between 600 and 800°C. One reason could be that the pH 6 sample contained more phenol or ether groups than the other samples. Another possibility is that one type of these surface groups was not present in the other samples except in sample pH 6. Lower pH values such as pH 6 could favor the presence of more acidic surface groups such as phenols or lactols[35], which decomposed as CO released in the 600-800 °C temperature region.

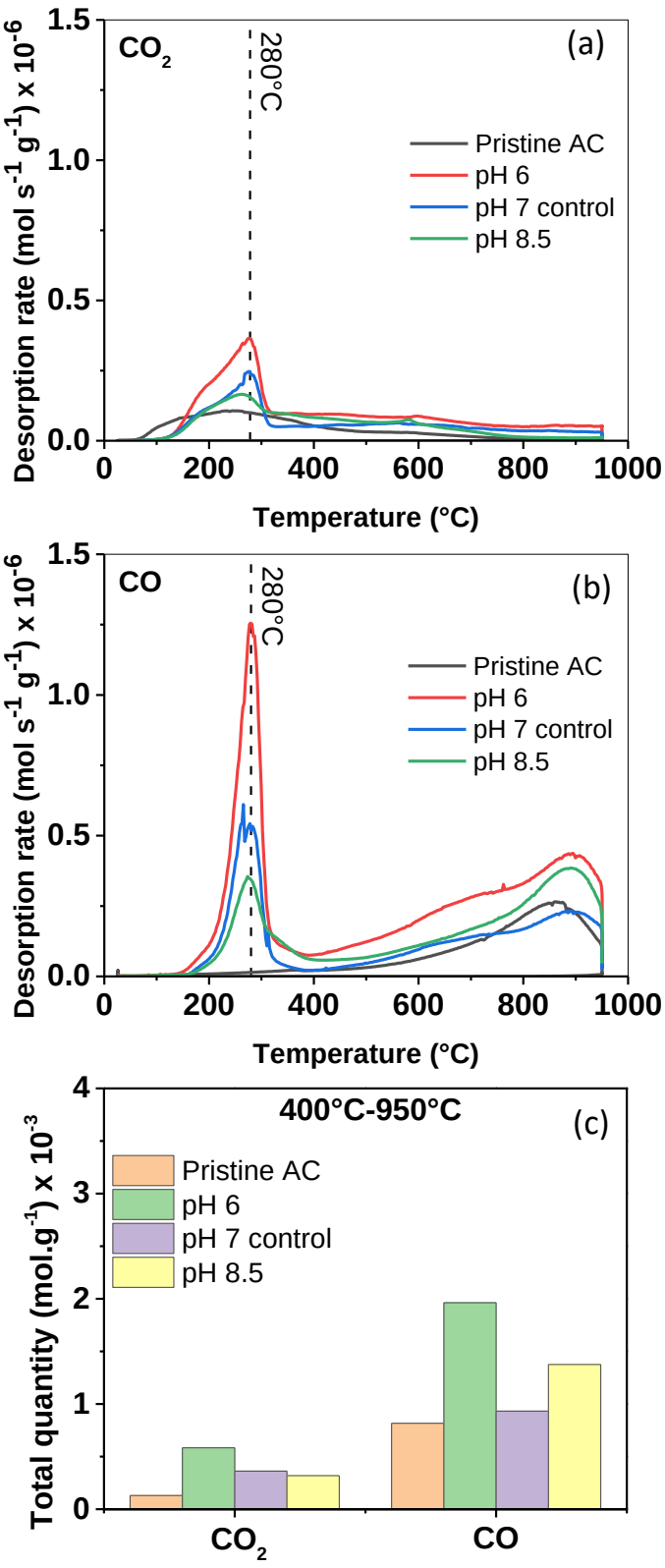

Figure 6. TPD-MS profiles of (a) CO and (b) CO_2 for activated carbons before and after adsorption of cya under different pH conditions; (c) total CO_2 and CO quantities evolved between 400°C and 950°C

Figure 6 (c) shows the total amount of CO and CO_2 per gram of sample, evolved between 400°C and 950°C. It can be seen that pH 6 has more oxygenated surface groups, which decomposed as CO and CO_2, and more acidic functions were also likely present, which could contribute to a better adsorption of cya.

To gain more insight into the possible interactions between the carbon surface and cya, we performed XPS studies after adsorption at different pH values. The high resolution N 1s XPS spectra of the samples performed at pH 6 and pH 8.5 compared to the pH 7 control are shown in Figure 7a-c. To track the presence of cya on the carbon surface, we could follow the possible interaction on the surface by examining at the change in the amount of the triazine ring. The two expected nitrogen states were visible with binding energies of approximately 400 eV. The triazine signature (C-N bond) appearing at 400 eV had the highest intensity and a behavior almost similar to that of the pH 6 and pH 7 control samples. However, for pH 8.5 the bond intensity was significantly lower. This observation was in good agreement with the TPD-MS m/z peak intensities as well. Furthermore, a small peak corresponding to the C=N bond appeared at 398 eV and was more intense for the pH 6 sample than for the control and pH 8.5 samples. An additional very small signature of the N^+-C bond was also observed for the pH 6 sample.

Figure S6 (SI) shows the C1s high resolution spectra and the presence of oxygen-functional groups (COOR, C=O, C-OR, C-C=O) and that of C – triazine bonds. If we compare the amount of functional groups associated with the energy level of C 1s, as shown in Figure 7d, there was a significant increase in the functionalities of C-triazine for samples with pH 6 > pH 7 control > pH 8.5. This observation also supported the quantified amount of cya of TGA WL2, which led to the conclusion that the pooltester equipment was less sensitive if the pH as varied from neutral to acidic or basic. Nevertheless, it was interesting to note that the acidic pH enhanced the cya capacity compared to the neutral or basic pH scenarios.

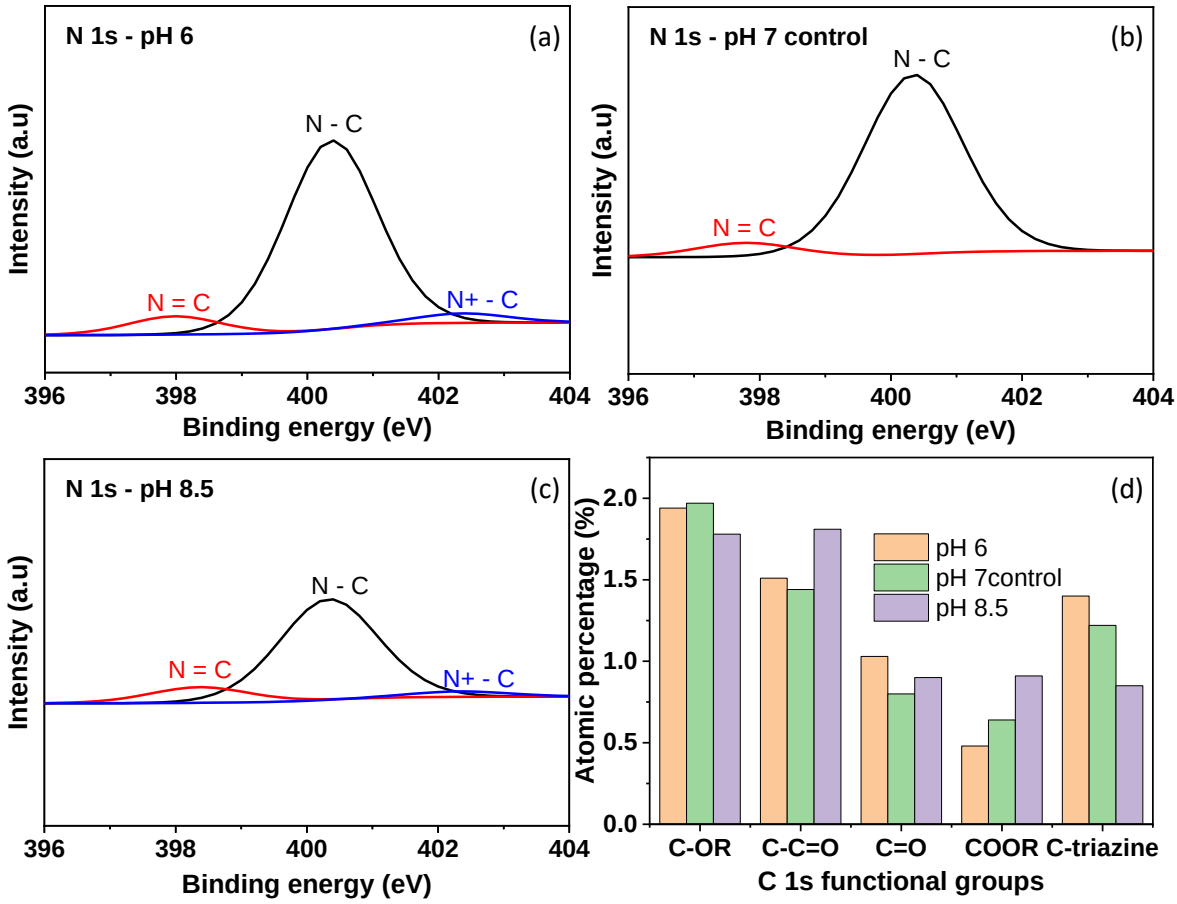

Figure 7. XPS analysis of activated carbon after cya adsorption under different pH. High resolution spectra of N 1s (a) at pH 6 (b) at pH 8.5 (c) at pH 7 control. (d) comparison between amounts of C 1s functional groups for adsorption performed under different pH conditions

The characterization of solid AC after the adsorption experiments revealed that substantial differences could be observed in the pooltester results when the liquid part was analyzed. This could cause an issue of reliability with such pooltesters when used in the swimming pool industry. To ensure that the concentration of cya obtained by the pooltester was reliable and to reduce the number of measurements, a more accurate analytical method is highly desirable. For this purpose, we optimized a UV-vis analysis methodology, as presented in the next section.

Reliability testing of pool testers by the UV-Vis method

Considering the inconsistency of pooltester measurements in some cases (1 aberrant measurement out of 3 or 4) we have tried to find an alternative method to quantify cya from solution using the UV-VIS technique.

For UV experiments, the pH of the resulting adsorption filtrate was adjusted to pH 8 (normal reaction pH is 7) using pH 8 buffer solution. We observed a strong absorbance band at 213 nm, which was similar to previously reported studies from the literature with a well-fitted calibration curve (Figure S2a,b) [36]. A minimum of three batches were performed for consistency and the results are expressed in Table 4 compared to the corresponding pooltester values. The UV-vis readings were found to be more consistent between batches with a lower standard deviation. Although the average adsorption capacity calculated was not much different for both methods, the UV-vis readings were more consistent and repeatable, contrary to the pooltesters. Thus, UV-vis spectroscopy could be implemented to accurately measure the cya concentration in water and to check the possible error range for pooltester equipment with fewer batches.

Table4. Comparison of cya adsorption capacity (mg/g) by the pooltester and UV-Vis analysis methods

Batch	Batch 4	Batch 5	Batch 6	Average
Pooltester (mg g^{-1})	115.3	144	80	113.1 ± 32
UV-Vis (mg g^{-1})	94	125.3	90.7	103.3 ± 19

To understand the effect of contact time on adsorption capacity, we examined different kinetic models by fitting the experimental data to corresponding linearized kinetic models. Adsorption kinetics help to describe the physical and chemical characteristics[37] of the adsorbent, which can be used to explain the surface phenomena occurring between the adsorbent and the adsorbate.

Figure 8a shows the evolution of cya adsorption on AC with contact time. As seen in the figure, the adsorption capacity gradually increased over time until reaching a maximum value. Almost 90 percent of the adsorption occurred within 8 hours (480 min) and then slowly approached e equilibrium after 16-24 hours and saturation occurred approximately 48 hours (2880 min). To better understand the mechanism, the experimental data were fitted to linear models of i) intraparticle diffusion (Figure S7b), ii) pseudo first order (Figure S7a) and iii) pseudo second order kinetics (Figure 8b).

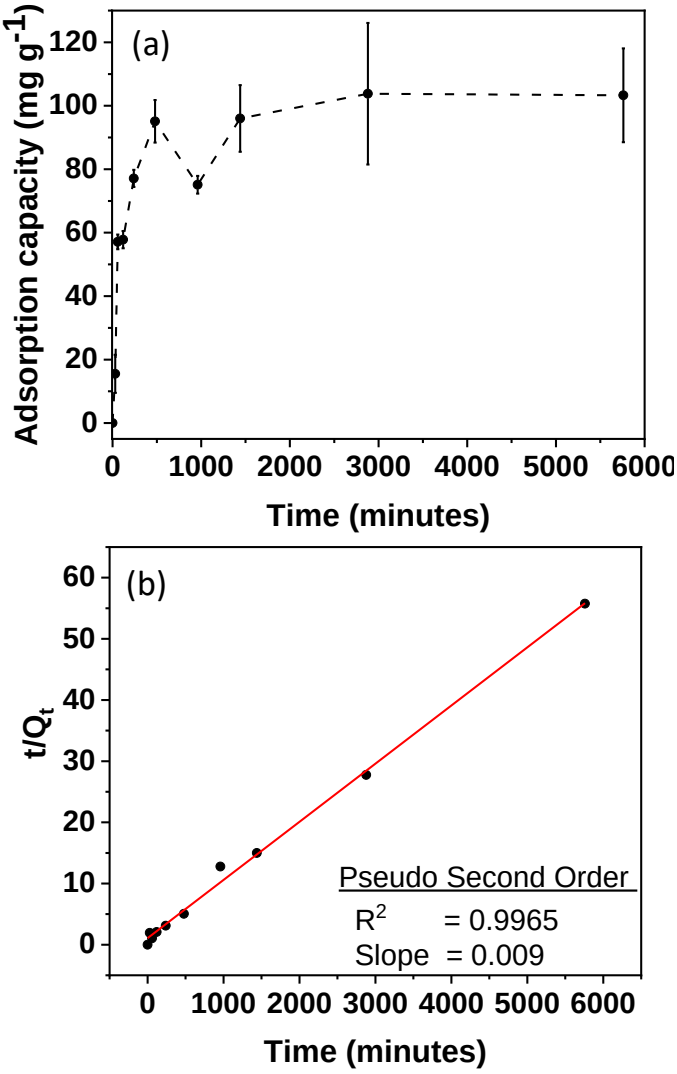

Figure 8. (a) Change in adsorption capacity with time and (b) linearized fit to pseudo second order kinetic model

The experimental data best fit the pseudo second order model as shown in Figure 8b and Table 5 with a regression of 0.9965. Pseudo second order kinetics signified that the rate limiting mechanism as mainly by chemisorption which controlled the entire adsorption process rather than physisorption or diffusion into the pores. Chemisorption involves valence forces through the sharing or exchange of electrons between an adsorbent and an adsorbate, and therefore the rate of desorption is negligible compared to the rate of adsorption.

Table 5. Linear fit of experimental data at pH 8 with different kinetic models

Kinetic Model	**Regression R^2**	**Rate constant, k**	**Q_e (mg/g)**
Pseudo first order	0.5410	0.072×10^{-3}	5.35
Pseudo second order	0.9965	1.15×10^{-3}	105.26
Intra-particle diffusion	0.5820	0.93	-

The available surface functional groups, mainly acidic groups as we observed, on AC provide various chemical interaction with cya from swimming pool water. As represented in Figure S8, these interactions include, hydrogen-bonding, electrostatic interactions, Π-Π interactions etc with cya molecule. The adsorption efficiency of AC is mainly controlled by these surface interactions, which can be determined by kinetic models as described above. As is evident, the main driving force for the adsorption of cya molecules on the surface is controlled by surface groups. These results agreed with the surface chemistry observed from the TPD-MS and XPS analysis. As a result, the pH of the reaction highly influenced the adsorption capacity of activated carbon toward cya.

In summary, the successful characterization of activated carbon and the adsorption behavior of cya open up some more promising experiments that could be beneficial for the future

perspective of the present study. A more in-depth adsorption study could be carried out using HPLC method. A systematic study of the effect on the surface chemistry of activated carbon including different acidic, basic groups (N- or S-based groups) and hydrophobic surfaces could also be promising. This might allow us to have a clear picture of the optimal surface chemistry required to enhance the adsorption capacity. The porosity of the carbon could also be adjusted, particularly the pore size which seems rather narrow for cya molecules that have a large size.

Conclusion

In this study, we systematically analyzed the physicochemical properties of activated carbon for the efficient adsorption of cya from water. The analysis showed that the physicochemical properties of activated carbon such as high specific surface area, optimal pore size, and oxygen-surface functionalities can be beneficial for efficiently capturing cya at the active surface sites by physisorption and chemisorption at the surface functional groups.

Batch adsorption tests were carried out and the activated carbon exhibited an adsorption capacity of 88.1±19.9 mg g^{-1}. The adsorbed molecule was quantified using conventional pooltester equipment and the TGA weight loss method and identified using TPD-MS analysis. Varying the pH of the adsorption test led us to conclude that an acidic pH enhanced the adsorption of cya onto activated carbon. The observations were confirmed with the help of TPD-MS by referring to m/z = 43 peak intensities. The high-resolution C 1s and N 1s spectra of the XPS spectra showed that the samples prepared at pH= 6 had more triazine bonds. These pH conditions could be implemented in swimming pools during the pH correction time for a practical benefit. Because the sensitivity of pool testing equipment decreases with a higher concentration of cya, the reliability of such equipment is limited. During this study, we developed a methodology to quantify cya more accurately using UV-vis spectroscopy. By maintaining a pH greater than 7.5, the UV-vis method could be effectively implemented to validate the accuracy of the pooltester method with better repeatability before being used for

research purposes. With the help of the UV-vis method, the effect of contact time vs. adsorption capacity of activated carbon was studied. The adsorption followed pseudo-second-order kinetics, suggesting that the chemisorption reactions between the carbon surface and cya mainly governed the adsorption processes. The TGA weight loss method and UV-Vis method can be used by swimming pool professional to have a more accurate quantification of residual cya for the research purposes.

Conflict of Interest

The authors declare no conflict of interest.

Supporting Information:

Resonance anionic structures of cya, UV-Vis absorbance spectra of cya, EDX spectra of AC, TGA under air of AC, Theoretical MS spectra of cya, High resolution XPS spectra of AC, Fit for adsorption of cya, cya adsorption mechanism

Acknowledgements

This project was funded by WATERAIR swimming pools Pvt. Ltd and Centre national de la recherche scientifique (CNRS). The authors thank Gautier Schrodj (TGA), Philippe Fioux (XPS), Jean-Marc Le Meins (XRD) and Adrian Beda (SEM and other laboratory procedures) for all technical support via IS2M technical platforms.

References

(1) Bonadonna, L.; La Rosa, G. A Review and Update on Waterborne Viral Diseases Associated with Swimming Pools. *Int. J. Environ. Res. Public Health* **2019**, *16* (2), 166. https://doi.org/10.3390/ijerph16020166.

(2) Borgmann-Strahsen, R. Comparative Assessment of Different Biocides in Swimming Pool Water. *Int. Biodeterior. Biodegrad.* **2003**, *51* (4), 291–297. https://doi.org/10.1016/S0964-8305(03)00040-4.

(3) Ilyas, H.; Masih, I.; Van der Hoek, J. P. Disinfection Methods for Swimming Pool Water: Byproduct Formation and Control. *Water* **2018**, *10* (6), 797. https://doi.org/10.3390/w10060797.

(4) Corral Bobadilla, M.; Vergara González, E. P.; Lostado Lorza, R.; Somovilla Gómez, F. Effecting Partial Elimination of Isocyanuric Acid from Swimming Pool Water Systems. *Water* **2019**, *11* (4), 712. https://doi.org/10.3390/w11040712.

(5) Canelli, E. Chemical, Bacteriological, and Toxicological Properties of Cyanuric Acid and Chlorinated Isocyanurates as Applied to Swimming Pool Disinfection: A Review. *Am J Public Health* **1974**, *64* (2), 155–162. https://doi.org/10.2105/AJPH.64.2.155.

(6) Wojtowicz, J. A. Effect of Cyanuric Acid on Swimming Pool Maintenance. J. Swimming pool Spa Ind. **2004**, 5 (1), 15-19.

(7) Falk, R. A.; Blatchley, E. R.; Kuechler, T. C.; Meyer, E. M.; Pickens, S. R.; Suppes, L. M. Assessing the Impact of Cyanuric Acid on Bather's Risk of Gastrointestinal Illness at Swimming Pools. *Water* **2019**, *11* (6), 1314. https://doi.org/10.3390/w11061314.

(8) Zdanovskaia, M. A.; Schwarz, C. E.; Habib, A. D.; Hill, N. J.; Esselman, B. J. Access to Computational Chemistry for Community Colleges via WebMO. *J. Chem. Educ.* **2018**, *95* (11), 1960–1965. https://doi.org/10.1021/acs.jchemed.8b00310.

(9) Sigmund, G.; Sun, H.; Hofmann, T.; Kah, M. Predicting the Sorption of Aromatic Acids to Noncarbonized and Carbonized Sorbents. *Environ. Sci. Technol.* **2016**, *50* (7), 3641–3648. https://doi.org/10.1021/acs.est.5b06033.

(10) Klotz, I. M.; Askounis, T. Absorption Spectra and Tautomerism of Cyanuric Acid, Melamine and Some Related Compounds. *J. Am. Chem. Soc.* **1947**, *69* (4), 801–803. https://doi.org/10.1021/ja01196a017.

(11) Liang, X.; Pu, X.; Zhou, H.; Wong, N.-B.; Tian, A. Keto–Enol Tautomerization of Cyanuric Acid in the Gas Phase and in Water and Methanol. *J. of Mol. Struct.: THEOCHEM* **2007**, *816* (1), 125–136. https://doi.org/10.1016/j.theochem.2007.04.010.

(12) Latta, D. Interference in Melamine–Based Determination of Cyanuric Acid Concentration. J Swimming pool Spa Ind. **1995**, 1 (2), 37-39

(13) Downes, C. J.; Mitchell, J. W.; Viotto, E. S.; Eggers, N. J. Determination of Cyanuric Acid Levels in Swimming Pool Waters by u.v. Absorbance, HPLC and Melamine Cyanurate Precipitation. *Water Research* **1984**, *18* (3), 277–280. https://doi.org/10.1016/0043-1354(84)90100-3.

(14) Cantú, R.; Evans, O.; Kawahara, F. K.; Shoemaker, J. A.; Dufour, A. P. An HPLC Method with UV Detection, PH Control, and Reductive Ascorbic Acid for Cyanuric Acid Analysis in Water. *Anal. Chem.* **2000**, *72* (23), 5820–5828. https://doi.org/10.1021/ac0005868.

(15) EHLING, S.; TEFERA, S.; HO, I. P. High-Performance Liquid Chromatographic Method for the Simultaneous Detection of the Adulteration of Cereal Flours with Melamine and Related Triazine by-Products Ammeline, Ammelide, and Cyanuric Acid. *Food addit. contam* **2007**, *24* (12), 1319–1325.

(16) Fiamegos, Y. C.; Konidari, C. N.; Stalikas, C. D. Cyanuric Acid Trace Analysis by Extractive Methylation via Phase-Transfer Catalysis and Capillary Gas Chromatography

Coupled with Flame Thermoionic and Mass-Selective Detection. Process Parameter Studies and Kinetics. *Anal. Chem.* **2003**, *75* (16), 4034–4042. https://doi.org/10.1021/ac030057e.
(17) Ghimbeu, C. M.; Gadiou, R.; Dentzer, J.; Schwartz, D.; Vix-Guterl, C. Influence of Surface Chemistry on the Adsorption of Oxygenated Hydrocarbons on Activated Carbons. *Langmuir* **2010**, *26* (24), 18824–18833. https://doi.org/10.1021/la103405j.
(18) Passé-Coutrin, N.; Maisonneuve, L.; Durimel, A.; Dentzer, J.; Gadiou, R.; Gaspard, S. Improving of Understanding of Beta-Hexachlorocyclohexane (HCH) Adsorption on Activated Carbons by Temperature-Programmed Desorption Studies. *Environ Sci Pollut Res* **2016**, *23* (1), 128–138. https://doi.org/10.1007/s11356-015-4759-1.
(19) Gadiou, R.; dos Santos, E. A.; Vijayaraj, M.; Anselme, K.; Dentzer, J.; Soares, G. A.; Vix-Guterl, C. Temperature-Programmed Desorption as a Tool for Quantification of Protein Adsorption Capacity in Micro- and Nanoporous Materials. *Colloids Surf B Biointerfaces* **2009**, *73* (2), 168–174. https://doi.org/10.1016/j.colsurfb.2009.05.012.
(20) Peredo-Mancilla, D.; Matei Ghimbeu, C.; Réty, B.; Ho, B.-N.; Pino, D.; Vaulot, C.; Hort, C.; Bessieres, D. Surface-Modified Activated Carbon with a Superior CH4/CO2 Adsorption Selectivity for the Biogas Upgrading Process. *Ind. Eng. Chem. Res.* **2022**, *61* (34), 12710–12727. https://doi.org/10.1021/acs.iecr.2c01264.
(21) *Standard Test Method for Determination of Contact pH with Activated Carbon*. https://www.astm.org/d6851-02r11.html (accessed 2023-06-14).
(22) Jagiello, J.; Olivier, J. P. 2D-NLDFT Adsorption Models for Carbon Slit-Shaped Pores with Surface Energetical Heterogeneity and Geometrical Corrugation. *Carbon* **2013**, *55*, 70–80. https://doi.org/10.1016/j.carbon.2012.12.011.
(23) *ASTM D7582-15 - Standard Test Methods for Proximate Analysis of Coal and Coke by Macro Thermogravimetric Analysis*. https://webstore.ansi.org/standards/astm/astmd758215 (accessed 2023-06-14).
(24) Brender, P.; Gadiou, R.; Rietsch, J.-C.; Fioux, P.; Dentzer, J.; Ponche, A.; Vix-Guterl, C. Characterization of Carbon Surface Chemistry by Combined Temperature Programmed Desorption with in Situ X-Ray Photoelectron Spectrometry and Temperature Programmed Desorption with Mass Spectrometry Analysis. *Anal.Chem.* **2012**, *84* (5), 2147–2153. https://doi.org/10.1021/ac102244b.
(25) Thommes, M.; Morlay, C.; Ahmad, R.; Joly, J. P. Assessing Surface Chemistry and Pore Structure of Active Carbons by a Combination of Physisorption (H2O, Ar, N2, CO2), XPS and TPD-MS. *Adsorption* **2011**, *17* (3), 653–661. https://doi.org/10.1007/s10450-011-9360-4.
(26) Tan, I. A. W.; Hameed, B. H.; Ahmad, A. L. Equilibrium and Kinetic Studies on Basic Dye Adsorption by Oil Palm Fibre Activated Carbon. *Chem. Eng. J.* **2007**, *127* (1), 111–119. https://doi.org/10.1016/j.cej.2006.09.010.
(27) Dandekar, A.; Baker, R. T. K.; Vannice, M. A. Characterization of Activated Carbon, Graphitized Carbon Fibers and Synthetic Diamond Powder Using TPD and DRIFTS. *Carbon* **1998**, *36* (12), 1821–1831. https://doi.org/10.1016/S0008-6223(98)00154-7.
(28) Figueiredo, J. L.; Pereira, M. F. R.; Freitas, M. M. A.; Órfão, J. J. M. Modification of the Surface Chemistry of Activated Carbons. *Carbon* **1999**, *37* (9), 1379–1389. https://doi.org/10.1016/S0008-6223(98)00333-9.
(29) Ryczkowski, J.; Pasieczna, S.; Figueiredo, J. L.; Pereira, M. F. R.; Borowiecki, T. Characterization of Activated Carbons by FT-IR/PAS and TPD. *J. Phys. IV France* **2004**, *117*, 57–63. https://doi.org/10.1051/jp4:2004117009.
(30) Masika, E.; Mokaya, R. Hydrogen Storage in High Surface Area Carbons with Identical Surface Areas but Different Pore Sizes: Direct Demonstration of the Effects of

Pore Size. *J. Phys. Chem. C* **2012**, *116* (49), 25734–25740. https://doi.org/10.1021/jp3100365.
(31) Raymundo-Piñero, E.; Kierzek, K.; Machnikowski, J.; Béguin, F. Relationship between the Nanoporous Texture of Activated Carbons and Their Capacitance Properties in Different Electrolytes. *Carbon* **2006**, *44* (12), 2498–2507. https://doi.org/10.1016/j.carbon.2006.05.022.
(32) Mangun, C. L.; Daley, M. A.; Braatz, R. D.; Economy, J. Effect of pore size on adsorption of hydrocarbons in phenolic-based activated carbon fibers. *Carbon*, **1998**, 36, 1 (2),123-129.
(33) Szymański, G. S.; Karpiński, Z.; Biniak, S.; Świątkowski, A. The Effect of the Gradual Thermal Decomposition of Surface Oxygen Species on the Chemical and Catalytic Properties of Oxidized Activated Carbon. *Carbon* **2002**, *40* (14), 2627–2639. https://doi.org/10.1016/S0008-6223(02)00188-4.
(34) Friedel Ortega, K.; Arrigo, R.; Frank, B.; Schlögl, R.; Trunschke, A. Acid–Base Properties of N-Doped Carbon Nanotubes: A Combined Temperature-Programmed Desorption, X-Ray Photoelectron Spectroscopy, and 2-Propanol Reaction Investigation. *Chem.Mater.* **2016**, *28* (19), 6826–6839. https://doi.org/10.1021/acs.chemmater.6b01594.
(35) Liu, Y.; Réty, B.; Matei Ghimbeu, C.; Soucaze-Guillous, B.; Taberna, P.-L.; Simon, P. Understanding Ageing Mechanisms of Porous Carbons in Non-Aqueous Electrolytes for Supercapacitors Applications. *J. Power Sources* **2019**, *434*, 226734. https://doi.org/10.1016/j.jpowsour.2019.226734.
(36) Yu, C.; Zhu, L.; Xiao, J.; Tang, H.; Guo, G.; Zeng, Q.; Wang, X. Ultrasonic Extraction and Determination of Cyanuric Acid in Pet Food. *Food Control* **2009**, *20* (3), 205–208. https://doi.org/10.1016/j.foodcont.2008.04.004.
(37) Dubinin, M. M. Fundamentals of the Theory of Adsorption in Micropores of Carbon Adsorbents: Characteristics of Their Adsorption Properties and Microporous Structures. *Pure Appl. Chem.* **1989**, *61* (11), 1841–1843. https://doi.org/10.1351/pac198961111841.